JOURNAL OF AIRCRAFT
Vol. 46, No. 2, March–April 2009

Computational Modeling of Variable-Droop Leading Edge in Forward Flight

Jeremy J. Bain,* Lakshmi N. Sankar,† J. V. R. Prasad,‡ and Oliver A. Bauchau§
Georgia Institute of Technology, Atlanta, Georgia 30332-0150
David A. Peters¶
Washington University, St. Louis, Missouri 63130
and
Chengjian He**
Advanced Rotorcraft Technology, Inc., Mountain View, California 94035

DOI: 10.2514/1.39174

In recent years, there has been significant interest in on-blade concepts that expand the operating envelope of helicopters without compromising the performance characteristics of the baseline rotor. The variable-droop leading-edge concept is explored in a modified version of the Navier–Stokes solver OVERFLOW. Modifications were made to the solver to allow deforming-grid capability. This concept was explored in dynamic stall tests of the VR-12 and SC1095 helicopter airfoils. The variable-droop leading-edge airfoils have dramatically reduced drag and moment rises associated with dynamic stall. Using the results of these tests, a modified UH-60A rotor incorporating variable-droop leading-edge airfoils was analyzed using loosely coupled computational fluid dynamics and comprehensive structural dynamics with OVERFLOW and DYMORE and compared with the standard UH-60A rotor for high-thrust-case flight 9017. Results show a reduction in the peak negative pitching moment. The rotor efficiency was shown to improve by 2.9% and the 4/rev component of vertical force reduced by 8%. These performance improvements can be improved with an improved droop schedule and by incorporating improved transonic airfoils.

Nomenclature

CCM^2	=	section chordwise-force coefficient $[C/(\frac{1}{2}\rho a^2 c)]$
CMM^2	=	section pitching-moment coefficient $[M/(\frac{1}{2}\rho a^2 c^2)]$
CNM^2	=	section normal-force coefficient $[N/(\frac{1}{2}\rho a^2 c)]$
C_T	=	thrust coefficient
c	=	chord
k	=	reduced frequency $(\omega c/2V_\infty)$
L/De	=	rotor lift per equivalent drag $[F_Z/(F_X - M_Z\Omega/V_\infty)]$
r/R	=	nondimensional radius
V_{tip}	=	rotor tip speed (ΩR)
V_∞	=	freestream velocity
μ	=	advance ratio $(V_\infty/V_{\text{tip}})$
σ	=	rotor solidity
ψ	=	rotor azimuth
Ω	=	main rotor rotation rate, rad/s

I. Introduction

RETREATING blade stall is a dominating factor in forward flight and can limit the operational envelope of a helicopter. In forward flight, the advancing blade encounters additional velocity due to the freestream and the retreating blade encounters a reduced velocity. This requires the same rotor span station to have good low-drag transonic and high-lift, low-speed performance. This represents a significant design compromise that results in airfoils that have lower performance than airfoils designed for each flow environment. In moderate-speed cruise flight ($\mu = 0.3$), the advancing blade has 3.45 times the dynamic pressure at the tip and 16 times at the midspan. To trim the aircraft, the lift generated on the advancing and retreating sides need to be balanced to avoid a large rolling moment. This requires the retreating blade to operate at or near its maximum lift capability while the advancing blade is at low or negative incidence. This causes the blade to undergo dynamic stall cycles as the blade goes from low to high incidence, causing large negative pitching moments, high vibration, and buffeting. The high negative pitching moment that occurs causes an elastic deformation that causes further pitch changes. These stall cycles limit the helicopter's maximum flight speed, maneuverability, and thrust of the aircraft.

A number of on-blade concepts have been proposed that offer tremendous potential for improved performance and reduced vibration for next-generation helicopters. These concepts attempt to improve aerodynamics on the retreating side while limiting their adverse effect on the advancing side. These include leading-edge slats [1,2], trailing-edge flaps [3–5], variable camber [6], and leading-edge deformation [7,8]. A number of active controls were applied to an Apache-like rotor in forward flight by Yeo [9] using CAMRAD II and modified airfoil tables. From these, the variable-droop leading edge (VDLE) was selected for further evaluation using two- and three-dimensional computational tests. A variable-droop leading edge has been shown in two-dimensional tests to greatly reduce the negative pitching-moment peak and peak drag, with small changes in lift in experimental and computational tests [10–12].

II. Numerical Methodology

A. OVERFLOW

The numerical simulations were done using the compressible Navier–Stokes computational fluid dynamics (CFD) code OVERFLOW [13]. OVERFLOW, developed by NASA, uses overset structured grids for a wide variety of problems, including rotorcraft simulations [14,15]. Version 2.0y with modifications made under the Defense Advanced Research Projects Agency's Helicopter Quieting Program, as reported by Duque et al. [16], was used with elastic blade motion capability. For 2-D calculations, two different grids were

Presented as Paper 3872 at the 4th Flow Control Conference, Seattle, WA, 23–26 June 2008; received 18 June 2008; accepted for publication 11 October 2008.

*Research Engineer, Aerospace Engineering. Student Member AIAA.
†Regents Professor, Aerospace Engineering. Associate Fellow AIAA.
‡Professor, Aerospace Engineering. Associate Fellow AIAA.
§Professor, Aerospace Engineering. Senior Member AIAA.
¶Professor, Mechanical Engineering, Campus Box 1185. Fellow AIAA.
**Vice President, Research and Development, 1330 Charleston Road. Senior Member AIAA.

generated. The first was a C-grid of dimensions 547×105, which was used with a $y+$ of 1. The second grid modeled the wind-tunnel walls with a smaller C-grid of dimensions 257×50 and a stretched 119×62 Cartesian grid similar to previous OVERFLOW runs in this wind tunnel [17,18]. In dynamic stall tests, 35,000 time steps per loop were used with 4 Newton subiterations. Calculations were made with up to 8 Newton subiterations and were found to produce near identical results. The solutions were run for 2–2.5 cycles using fourth-order central differencing and the kinetic-eddy simulation turbulence model [19,20]. Three-dimensional runs were made using a coarse $125 \times 82 \times 33$ node UH-60A blade C-grid. The first offbody grid used spacing of 0.2 times the tip chord. The entire grid used approximately 4.6 million grid points. OVERFLOW used 20 time steps per degree of azimuth, the detached-eddy simulation based on the Spalart–Allmaras turbulence model [21,22], and fourth-order central differencing.

B. OVERFLOW-DYMORE Coupling

For three-dimensional modeling, the UH-60A Blackhawk rotor was used. Analysis of helicopter rotors in forward flight is a complex multidisciplinary problem. Rotor blades are flexible beams that undergo significant elastic deflection. To solve the elastic deflections and trim the rotor to the required thrust, rolling, and pitching moment, several comprehensive structural dynamics (CSD) codes have been developed. The features and development history of these codes are summarized in [23]. They require the sectional structural properties of the rotor blade and details of the hub system. These properties determine the elastic characteristics of the rotor and interact with the aerodynamic forces. Accurate modeling of the aerodynamics of rotors is extremely challenging due to the requirement to model unsteady transonic flow with shocks, dynamic stall, reversed flows, and wakes. CSD codes rely on simplified aerodynamics from table lookups, stall models, and wake models. The aerodynamic calculations can be improved using a CFD code to supplement the internal aerodynamic calculation through CFD-CSD coupling, but at an approximately 2- or 3-order-of-magnitude increase in computational cost. Extensive work has been done on the UH-60A rotor using CFD-CSD coupling with a variety of solvers through the UH-60A Airloads Program [24]. Potsdam et al. [25] used loose coupling with OVERFLOW and CAMRAD II for a variety of level-flight conditions. OVERFLOW has also been used with other structural solvers, including RCAS [26] and DYMORE [16].

DYMORE [27] is a finite element solver that uses a multibody dynamics approach for the modeling of the rotor as a nonlinear elastic multibody system. A four-bladed UH-60A rotor model is used that includes the blades, lag dampers, and push rods. A dynamic wake is used for the initial aerodynamics. An autopilot algorithm is used to trim the rotor to the prescribed thrust and moment targets. This model has been used in previous studies using OVERFLOW [16] and GT-HYBRID [28]. No changes were made to the DYMORE model to account for the VDLE mechanical device.

A loose-coupling trim method initially developed by Tung et al. [29] was used and shown in Fig. 1. DYMORE is first run using lifting-line aerodynamics for several revolutions to obtain the trim solution and blade motions. The elastic blade motions are then transferred to OVERFLOW. The three forces and three moments in the hub frame are then calculated by OVERFLOW. This avoids any differences in the local frame due to changes in chord length and orientation that occur when the leading edge is deformed. Airloads and elastic deformations were calculated at 81 rotor stations. The first exchange of airloads from OVERFLOW to DYMORE took place after a periodic solution was obtained from two full rotor revolutions. Subsequent iterations passed airloads after two or three quarter-revolutions. Because airloads are exchanged at every degree of azimuth, care is required to ensure that the OVERFLOW loads have reached periodicity, to avoid discontinuities. DYMORE uses the OVERFLOW loads and applies a small trim correction using table-lookup aerodynamics. Typically, 6–10 iterations are required to converge to the desired thrust, rolling, and pitching moment. DYMORE ran for approximately 4 h per iteration. OVERFLOW was run on an 8-node 2.4 GHZ AMD Athlon processor cluster on 3–16 processors. Approximately 8 h per revolution are required when using 16 processors.

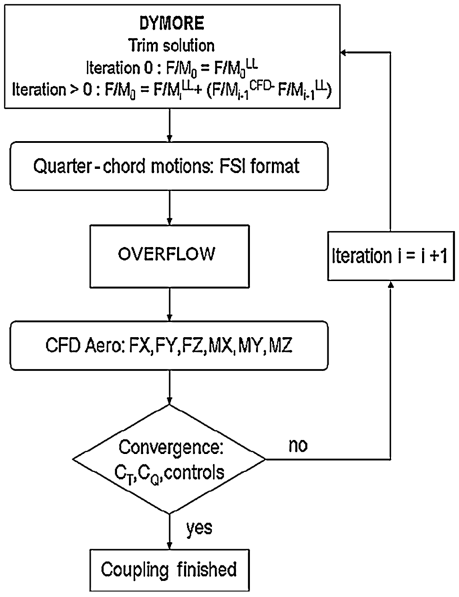

Fig. 1 Loose coupling CFD/CSD methodology (FSI denotes the fluid/structural interface).

C. Grid Deformation

Two different grid deformation techniques were implemented within OVERFLOW. The first method requires several volume grids to be created before running OVERFLOW. OVERFLOW was modified to read in four grids representing no-droop, maximum-droop, and two intermediate-droop values. The grid at each time step was then calculated algebraically by interpolating between those grids for a particular droop angle. The second method used followed that of Morton et al. [30]. This method was used by previous researchers for similar variable leading-edge deformations in OVERFLOW [11]. Once the deformed surface is calculated, the points in the normal direction are found by calculating the local normal to the grid surface. This maintains grid orthogonality at each time step. As the distance from the surface increases, a cubic spline is used to smoothly blend the deformed grid and the original grid. This maintains the outer boundary of the original grid. This results in some curving of the grid, as shown in Fig. 2. No differences were seen in the computed results to plotting accuracy. The second method has reduced memory requirements (as only the four surface grids were kept in memory instead of all four volume grids) and a small increase in computational time of 5%. In the three-dimensional tests, the original grid was modified with the leading-edge deformation at each time step before the elastic deformations were applied. The cubic blending function was modified for the 3-D grids to be fully blended at 0.5 chord lengths from the blade surface.

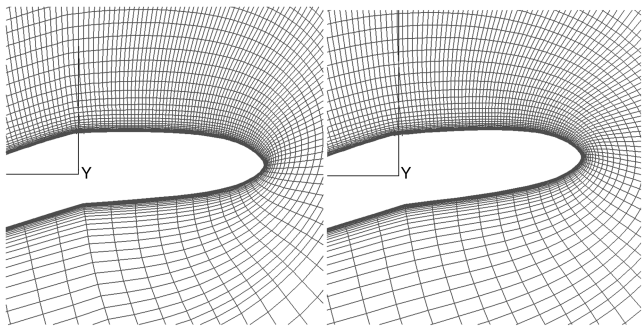

Fig. 2 Grid deformation using Morton scheme (left) and algebraic (right) (every second point shown).

III. Two-Dimensional Computations

To evaluate the grid deformation scheme in two dimensions, calculations were first done on a VR-12 airfoil with both fixed- and variable-droop leading edges from the experiment of Chandrasekhara et al. [10]. This experiment used a VR-12 airfoil with up to a 25 deg leading-edge droop from the quarter-chord. C-grids were made for fixed-droop angles of 0, 5, 10, 15, and 20 deg by rotating the leading-edge down, as shown in Fig. 3. The experiment has two mild steps near the hinge line, as the airfoil transitions between the leading-edge element, hinge, and main airfoil element resulted in some additional separation. The grid had a smooth upper surface and did not have these transitions.

Typically, dynamic stall computations use a single grid to model the entire flowfield and apply freestream boundary conditions in the far field. This yields good results when the wind tunnel has a high height-to-chord ratio so that the wind-tunnel walls can be neglected. Previous computations neglected the wind-tunnel-wall effects and underpredicted the lift-curve slope and delayed stall [12,31]. Figure 4 shows the VR-12 in dynamic stall with and without the wind-tunnel walls. The inclusion of wind-tunnel walls results in significant improvement of the lift-curve slope, maximum lift, and angle of stall of the baseline airfoil. Peak lift and drag were well predicted, but peak pitching moment was underpredicted. Figure 5 shows the lift results for 10 and 20 deg fixed-droop cases. Both show good agreement with experimental data when wind-tunnel walls are included. As the angle of droop is increased, the maximum lift, pitching moment, and drag are reduced.

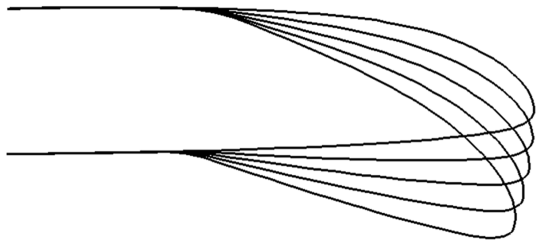

Fig. 3 Surface of VR-12 standard and drooped airfoils.

Next, the VDLE airfoil was tested. The droop schedule is such that the first quarter-chord of the airfoil is always at a 0 deg angle of attack. The results with and without the wind-tunnel walls are shown in Fig. 6. The inclusion of wind-tunnel walls improves the prediction of the lift-curve slope, but there is a steady offset of lift equal to the lift of the baseline airfoil at 0 deg. At a 0 deg angle of attack, the VDLE airfoil has the same shape as the baseline VR-12. The computed results for the VDLE airfoil show similar lift values at a low angle of attack to the baseline VR-12, but the experimental results have a near-zero value. The pitching moment at a high angle of attack is strongly underestimated.

Mach contours are compared at 18.5 deg on the upstroke in Fig. 7. As in the experiment, there is a small pocket of supersonic flow on the baseline airfoil, but the shock is not strong enough to cause separation. The maximum Mach number for the VDLE airfoil is

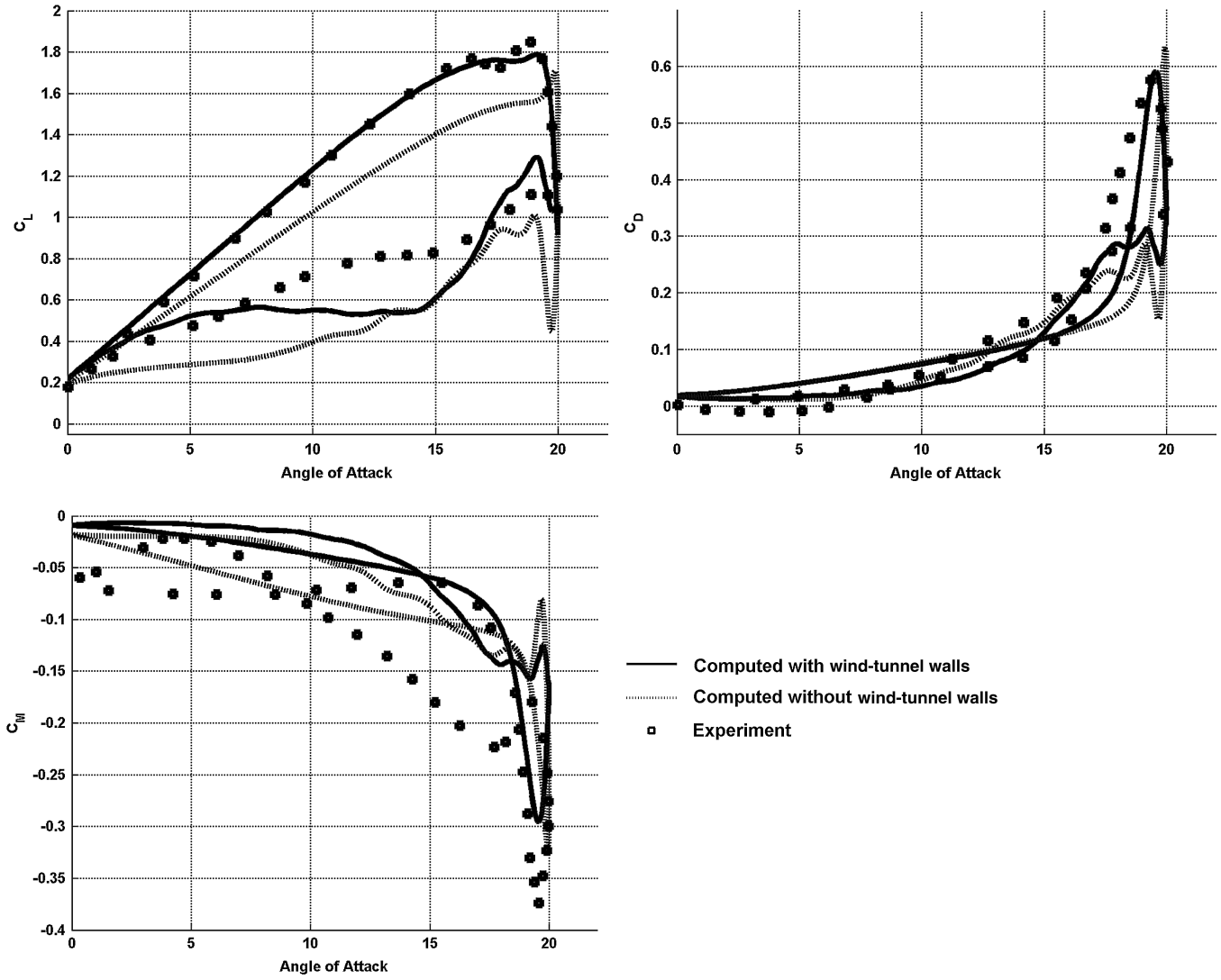

Fig. 4 Comparison of experimental and computed results for VR-12 $M = 0.3, k = 0.1$, and $\alpha = 10\,\text{deg} + 10\,\text{deg}\sin(\omega t)$.

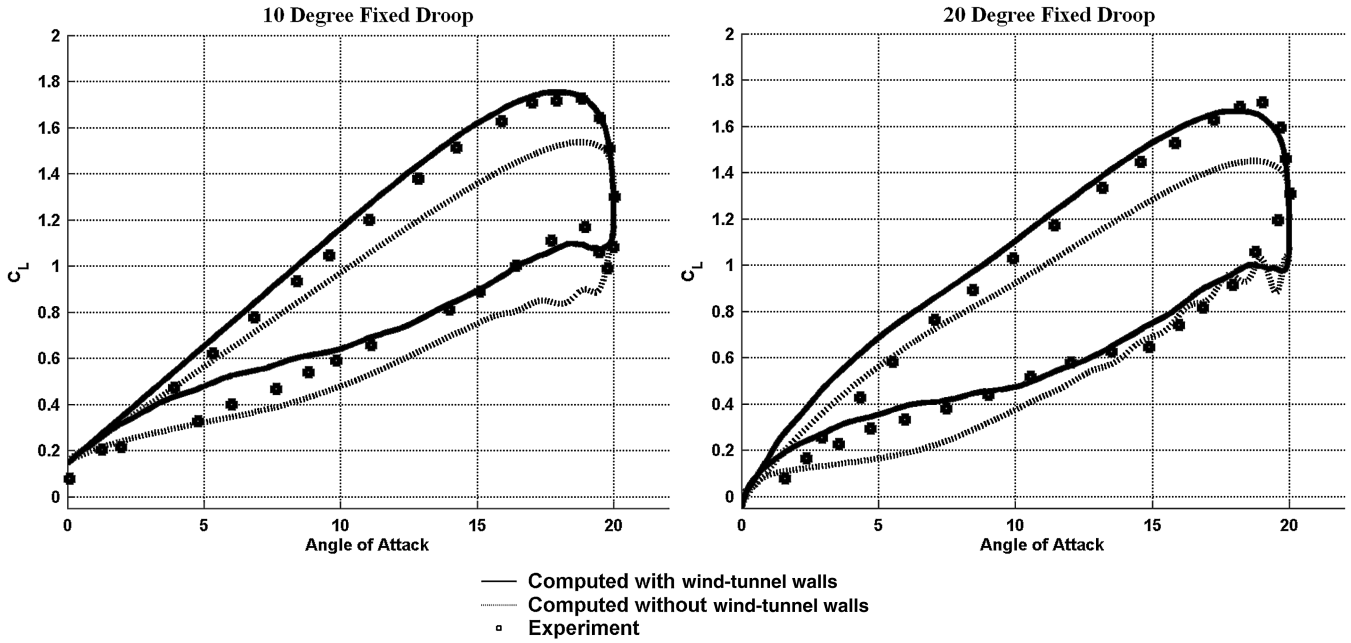

Fig. 5 Comparison of experimental and computed results for fixed droop VR-12 $M = 0.3$, $k = 0.1$, and $\alpha = 10\,\text{deg} + 10\,\text{deg}\sin(\omega t)$.

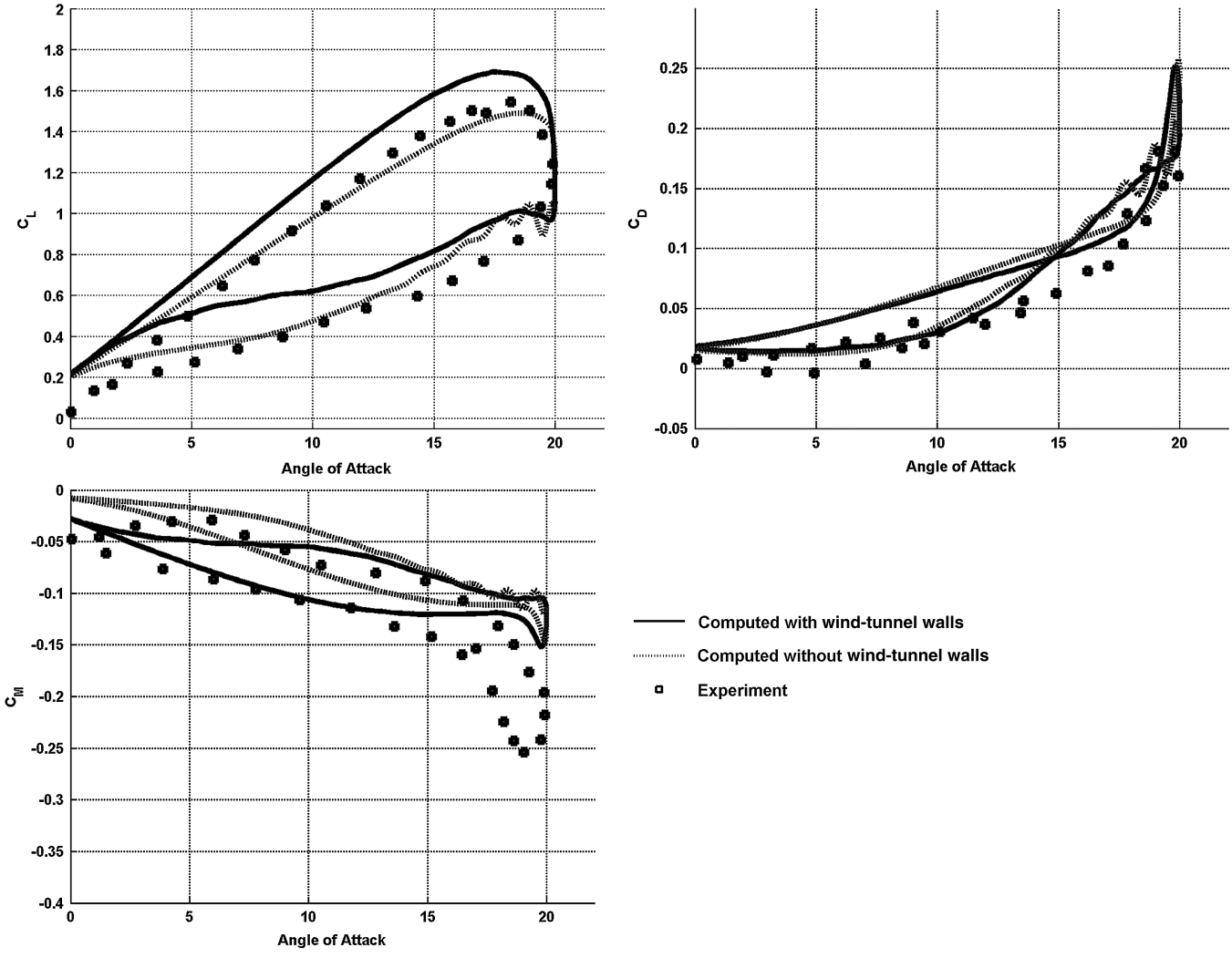

Fig. 6 Comparison of experimental and computed results for the VDLE airfoil $M = 0.3$, $k = 0.1$, and $\alpha = 10\,\text{deg} + 10\,\text{deg}\sin(\omega t)$.

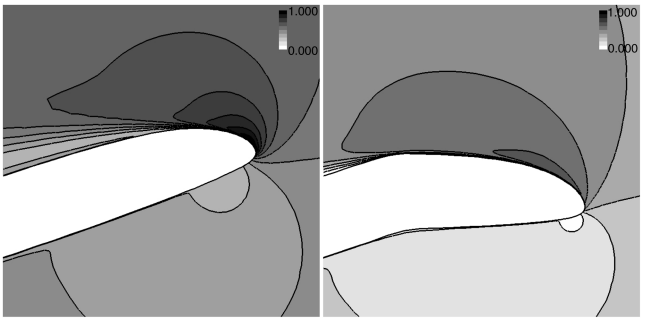

Fig. 7 Mach contours of VR-12 (left) and VDLE (right) at 18.5 deg on upstroke.

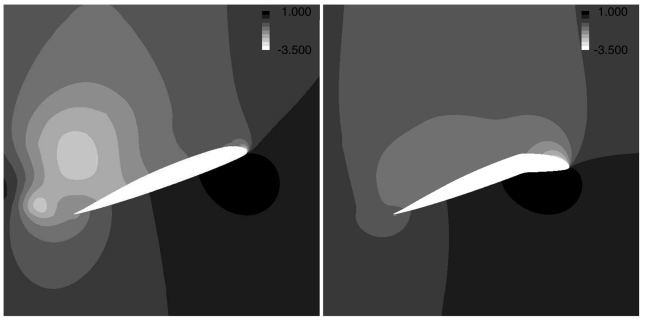

Fig. 8 C_P distribution of VR-12 (left) and VDLE (right) at 19.5 deg on upstroke.

significantly reduced from 1.063 to 0.642. The leading edge of the VDLE airfoil is at low incidence and has a much weaker $C_{P\min}$ of −3.16 than the −8.38 of the baseline airfoil. The C_P distribution at 19.5 deg is shown in Fig. 8. The dynamic stall vortex evident in the baseline image has been suppressed by the VDLE airfoil. The effect of the VDLE airfoil on peak lift, drag, and moment are summarized in Table 1. The VDLE has significant decreased the peak drag and pitching moment with minor reduction in peak lift.

Next, the SC1095 airfoil was simulated. This and the similar SC1094 airfoil are the airfoils on the UH-60A Blackhawk. There is a large database of computed and experimental results of this rotor for validation and comparison. The VR-12 is a more modern airfoil than the SC1095, with higher maximum lift-and-drag divergence Mach number. Results for the SC1095 in dynamic stall computations are shown in Figs. 9–11. The VDLE droop schedule was designed to maximize the $L^{3/2}/D$ on the upstroke using the results of the previous fixed-droop runs, as shown in Fig. 12. The schedule maintains the baseline SC1095 airfoil from 0 to 5 deg and then transitions to a 15 deg droop while keeping the angle of attack of the leading edge at 5 deg. The effect of the VDLE airfoil on peak lift, drag, and moment are summarized in Table 2. The results are similar to the VR-12 tests, except that the SC1095 shows an even greater computed drag reduction of 72 vs 57% for the VR-12. Figure 13 shows that the VDLE airfoil has successfully suppressed the leading-edge separation that characterizes dynamic stall. The flow characteristics are very similar to the VR-12 tests. The lower incidence of the leading edge of the VDLE airfoil maintains attached flow even at very high angle of attack. Some separation does occur near the trailing edge of the main airfoil element, but this region is significantly smaller than the baseline airfoils.

Table 1 Effect of VDLE VR-12 airfoil on critical quantities

	Experiment	Computed
Peak C_L reduction	8%	5%
Peak C_D reduction	63%	57%
Peak C_M reduction	31%	49%

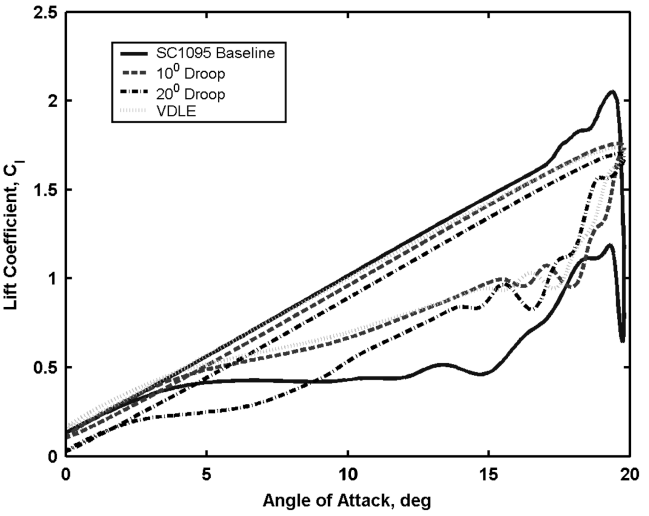

Fig. 9 SC1095 lift with drooped airfoils $M = 0.3$, $k = 0.1$, and $\alpha = 10\,\text{deg} + 10\,\text{deg}\sin(\omega t)$.

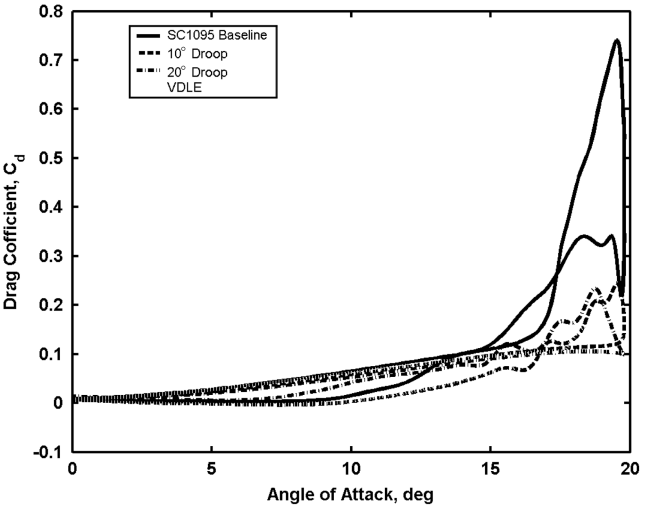

Fig. 10 SC1095 drag with drooped airfoils $M = 0.3$, $k = 0.1$, and $\alpha = 10\,\text{deg} + 10\,\text{deg}\sin(\omega t)$.

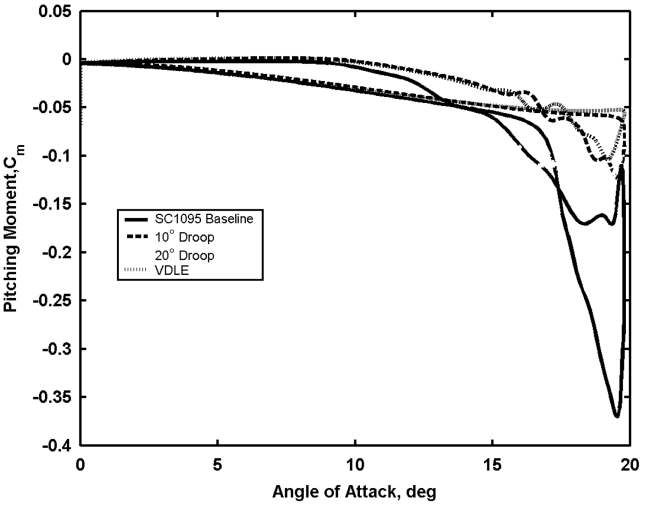

Fig. 11 SC1095 moment with drooped airfoils $M = 0.3$, $k = 0.1$, and $\alpha = 10\,\text{deg} + 10\,\text{deg}\sin(\omega t)$.

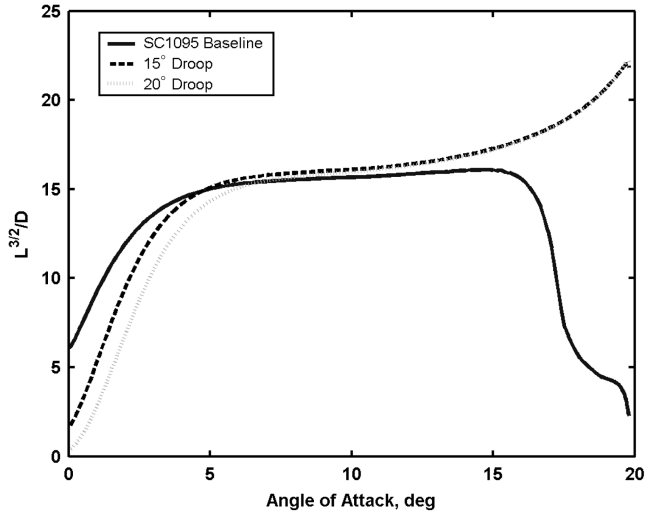

Fig. 12 SC1095 effect of droop on $L^{3/2}/D$.

IV. UH60A-Based Computations

For the UH-60A-based computations, flight C9017 was used. This is a moderate-speed (advance ratio $\mu = 0.237$) high-thrust ($C_T/\sigma = 0.129$) case that has two dynamic stall cycles. The two stalls occur at approximately $\psi = 270$ and 330 deg. The first stall is due to the high control angles necessary for the high thrust and the second stall is caused by the elastic deformation due to the torsion dynamics [32]. The standard UH-60A rotor was run for seven CFD-CSD coupling iterations to converge to the desired thrust, rolling-moment, and pitching-moment targets. The results are similar to results report by Potsdam et al. [25], except these computations use a coarser grid that does not capture all the events. The results are compared with experimental data in Figs. 14–16 at several span stations. The first stall is slightly underpredicted, which leads to a significant underprediction of the second stall. Because of the coarse offbody grid spacing of 0.2 chords, the wake is significantly dissipated, resulting in loss of the high-frequency content in the aft portion of the rotor disk. It has been previously noted that the integrated thrust is 13% higher than the measured thrust [25]. The pitching moments are plotted with the mean removed to eliminate the effect of steady-state offset.

Table 2 Effect of VDLE SC1095 airfoil on critical quantities

Peak C_L reduction	15%
Peak C_D reduction	72%
Peak C_M reduction	58%

A droop schedule was designed to reduce the effect of the two stalls on the outer portion of the rotor. The extent of the VDLE airfoil part of the blade was limited to 25% of the span from $r/R = 0.7$ to 0.95. The minimum feasible amount of time for the actuator to go from no deflection to a maximum of 15 deg was taken from a requirement for a VDLE mechanical system from a U.S. Army Small Business Innovation Research solicitation that specified that the mechanism must be capable of 5/rev motion [33]. The droop schedule was implemented using a slower 4/rev motion that began to droop at $\psi = 220$ deg, achieving a maximum of 15 deg droop at $\psi = 265$ deg. A maximum droop of 15 deg was chosen based on the SC1095 computations. The leading edge returns to the undeformed shape from $\psi = 305$ to 350 deg, as shown in Fig. 17.

The VDLE-based rotor was run for seven CFD-CSD coupling iterations to converge to the thrust, rolling-moment, and pitching-moment targets. The total and elastic pitches at the tip of the rotor blade are shown in Fig. 18. The pitch is nearly identical on the advancing side, as the collective and cyclic values are within 0.1 deg

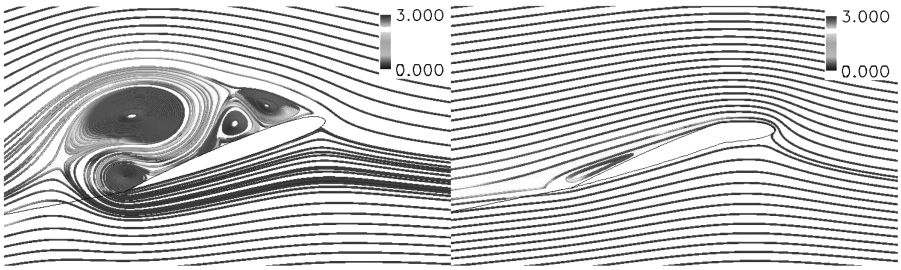

Fig. 13 Instantaneous streamlines around baseline SC1095 (left) and VDLE (right) at 19 deg on upstroke colored by vorticity.

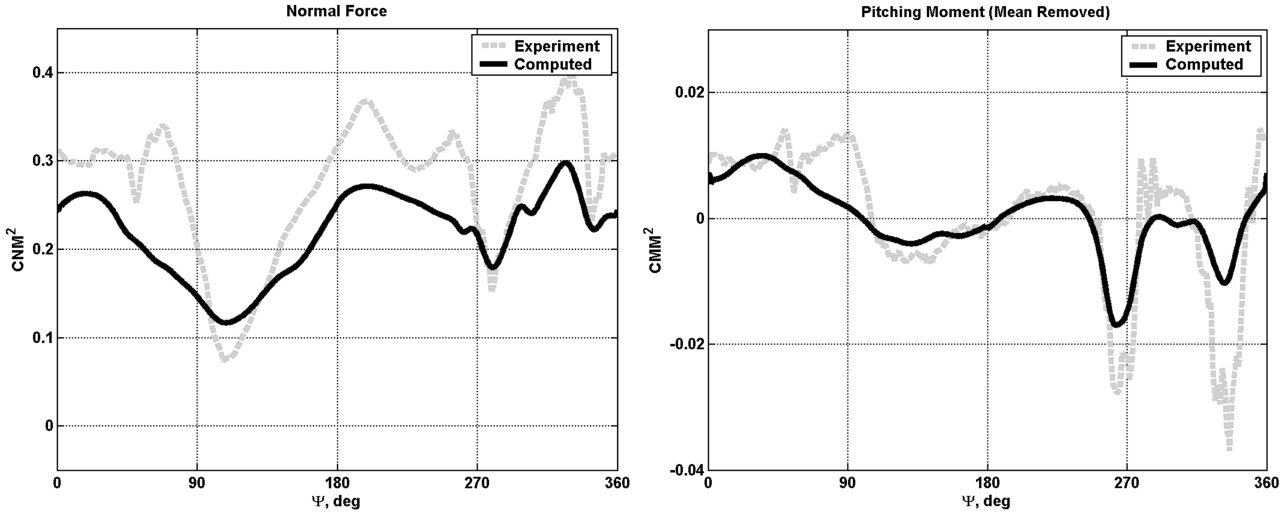

Fig. 14 Sectional loads at $0.865r/R$.

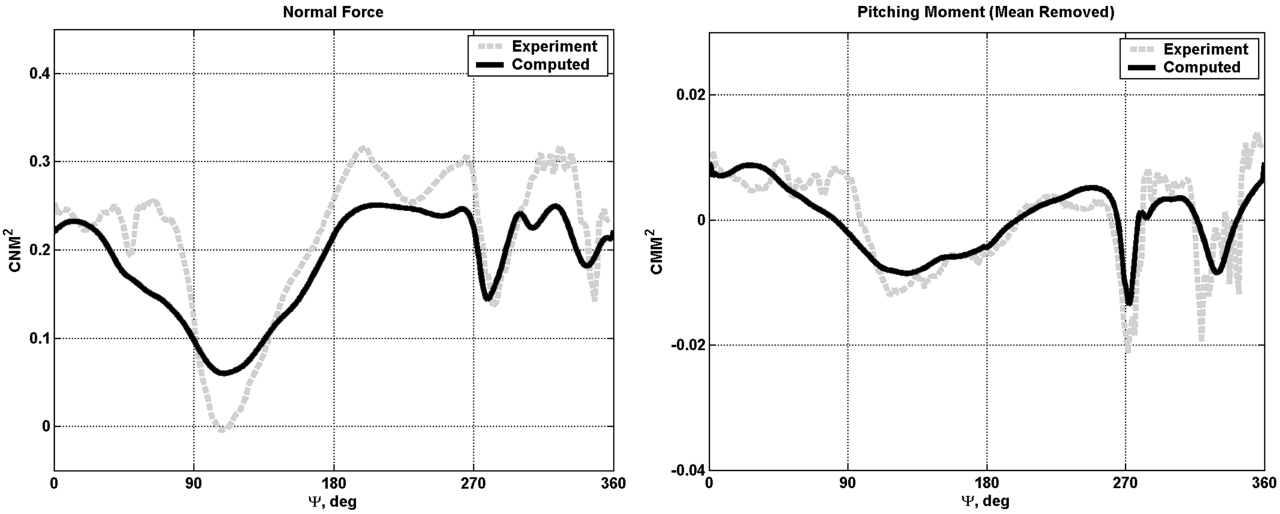

Fig. 15 Sectional loads at $0.920r/R$.

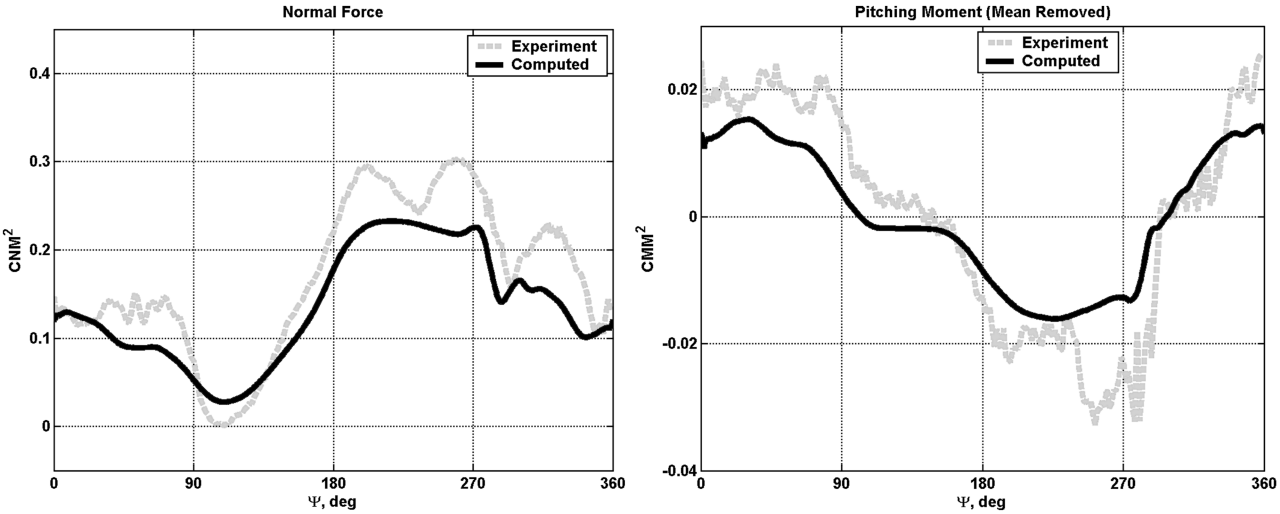

Fig. 16 Sectional loads at $0.990r/R$.

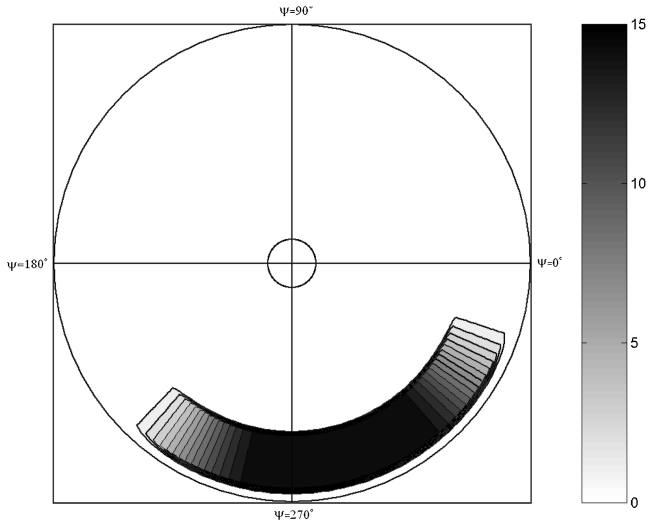

Fig. 17 Droop schedule implemented for C9017.

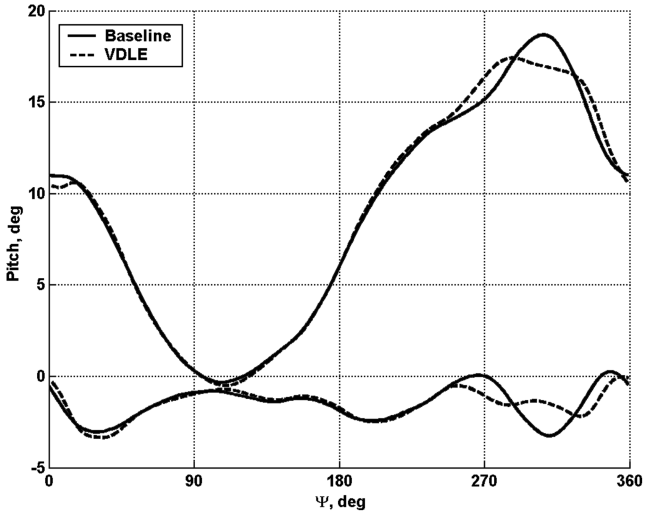

Fig. 18 Comparison of total and elastic pitch at tip of blade for the baseline and VDLE rotor.

of each other. The VDLE section has an increased nose-down pitching moment when the VDLE section begins to droop at $\psi = 220$ deg, and the maximum pitch at the tip at $\psi = 305$ deg is reduced by nearly 2 deg. Because of the elastic nature of rotor blades, the increased pitching moment in the VDLE section when it begins to droop affects the pitch of the entire blade. Figures 19–21 show the results for sectional pitching-moment, normal-force, and chordwise-force polar plots. The discontinuity in the loads at $r/R = 0.7$ and 0.85 is due to the increased chord with the tab. Figure 22 shows the local sectional loads at $r/R = 0.9$. The advancing side of the rotor for both cases is very similar, with only slight differences in the trim state. The VDLE-based rotor increases the pitching moment when it begins to droop at $\psi = 220$ deg, but the large spike in moment in the baseline rotor at $\psi = 270$ deg from the dynamic stall has been eliminated. The magnitude of the second stall has also been reduced. From the polar plot, a higher pitching moment is evident over the wide area in which the rotor droops, but maximum magnitude has been reduced. The pitching moment is significantly increased and the normal force is decreased for the VDLE blade around $r/R = 0.7$, where the VDLE section begins. This indicates that the leading edge has drooped too much at this span station and that the VDLE section does not need to extend this far inboard. Experimental data near this region show that a stall begins around 220 deg that was not captured in the baseline computations.

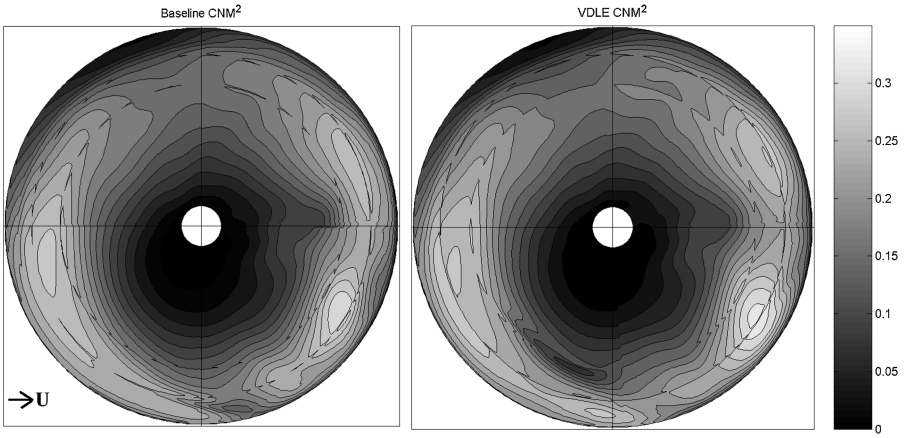

Fig. 19 Local normal-force polar plots.

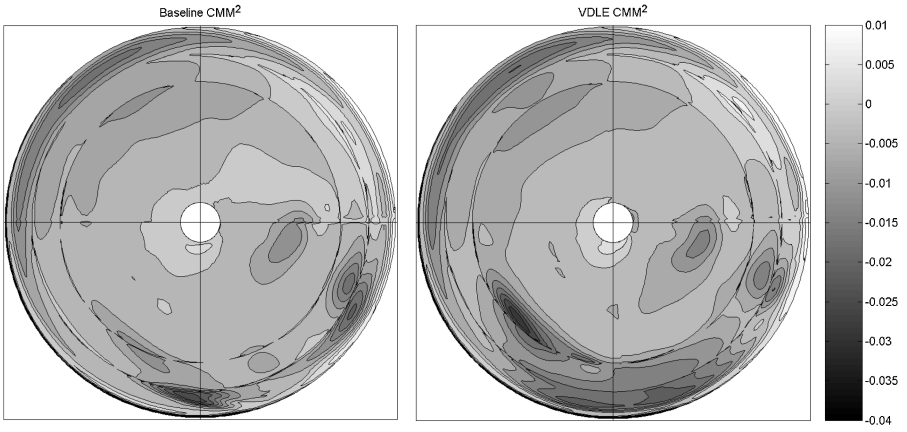

Fig. 20 Local pitching-moment polar plots.

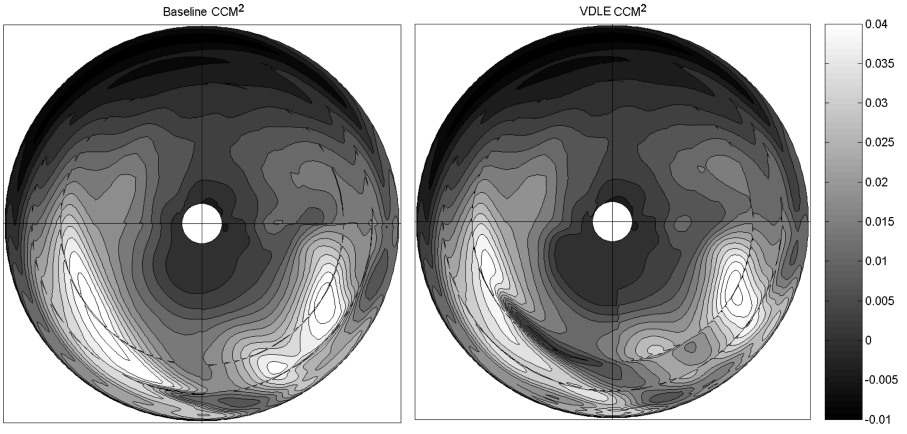

Fig. 21 Local chordwise-force polar plots.

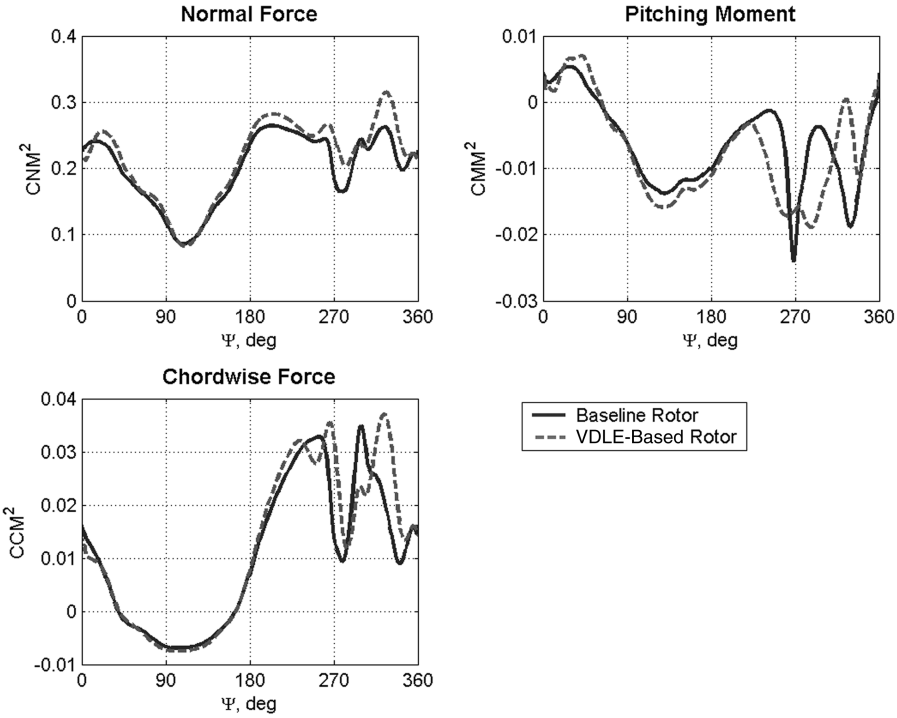

Fig. 22 Sectional loads forces at $r/R = 0.9$.

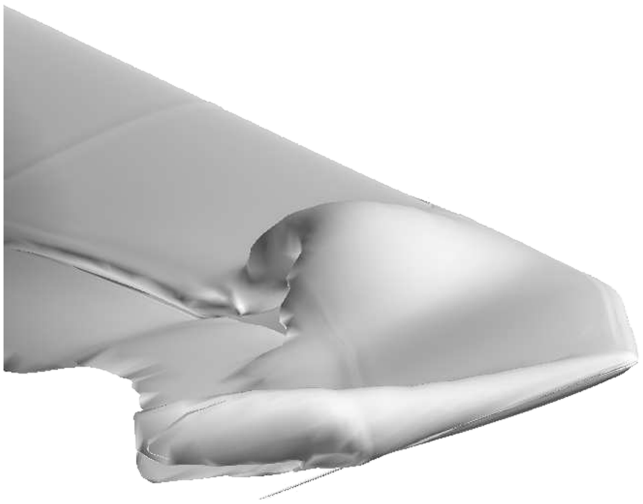

Fig. 23 Isosurface of constant vorticity at $\psi = 270$ deg on the baseline UH-60A blade.

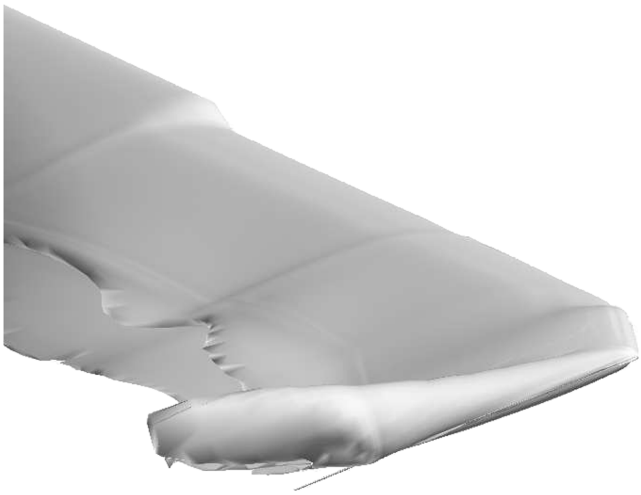

Fig. 24 Isosurface of constant vorticity at $\psi = 270$ deg on the VDLE-based UH-60A blade.

The effect of the VDLE blade on the stall at $\psi = 270$ deg is shown in Figs. 23 and 24 using an isosurface of constant vorticity. The baseline blade has a large pocket of separated flow on the upper surface of the blade that is not present for the VDLE blade. The vorticity for the VDLE blade is confined to the tip vortex and over the attached boundary layer. The flow remains attached or very mildly separated over the entire rotor disk for the VDLE blade.

The two rotors were compared using the effective lift-to-drag ratio L/De [34]. The VDLE-based rotor had a 2.9% improved L/De of 3.49 from 3.39 of the baseline rotor. This is mainly due to a 3.3% reduction in the torque required to power the main rotor. The edge force of the VDLE-based rotor was less than the baseline rotor, resulting in less propulsive force.

It is instructive to examine how the effect of the VDLE airfoil on local pitching moment and normal force affects the vibration. A primary contributor to vibration is the 4/rev vertical-force component. The VDLE blade had a 7.96% reduction in 4/rev vertical-force component. A 4/rev motion of the VDLE section of the blade for the entire rotor disk could potentially significantly reduce the vibration.

V. Conclusions

The OVERFLOW Navier–Stokes CFD code version 2.0y has been modified to allow for a leading-edge deformation. Two variable-droop leading-edge (VDLE) airfoils were analyzed in deep compressible dynamic stall. The leading edge changes to have low local incidence to the incoming flow at a high angle of attack. The leading-edge separation is suppressed, thereby greatly reducing the peak pitching moment and drag. The moderate-speed, high-thrust UH-60A C9017 flight was analyzed with the baseline rotor and a VDLE-based rotor. The VDLE-based rotor was able to maintain attached flow and reduced the peak pitching moment associated with dynamic stall. The pitching moment was increased over most of the area with the VDLE airfoil. The rotor efficiency improved by 2.9%, torque was reduced by 3.3%, and the 4/rev component of vertical

force was reduced by 8%. These performance improvements could likely be increased with an improved droop schedule. The improved retreating-blade performance with the VDLE allows for a better transonic airfoil to be used that could result in improved performance on the advancing side, further improving overall performance gains. Future work will likely include improving the pitching-moment prediction in separated flows, optimization of the droop schedule, optimizing the spanwise and chordwise extents of the VDLE airfoil, and examining high-speed flight.

Acknowledgments

This work was funded by NASA Cooperative Agreement NNX07AP33A, entitled "Flight Mechanics and Control Oriented Modeling for Next Generation On-Blade Control Concepts," with Wayne Johnson as Technical Monitor. We would like to thank Bob Kufeld for providing the UH-60A data. This work expands on tools developed under the Defense Advanced Research Projects Agency's Helicopter Quieting Project sponsored by Dan Newman. The authors would like to thank Alan Egolf of Sikorsky Aircraft Corporation for helpful comments and suggestions. The authors would also like to thank Eric Lynch at Georgia Institute of Technology for use of his coupling and postprocessing scripts.

References

[1] Carr, L. W., Chandrasekhara, M. S., Wilder, W. C., and Noonan, K. W., "Effect of Compressibility on Suppression of Dynamic Stall Using a Slotted Airfoil," *Journal of Aircraft*, Vol. 38, No. 2, Mar–Apr. 2001, pp. 296–309. doi:10.2514/2.2762

[2] Yu, Y. H., Lee, S., McAlister, K. W., and Tung, C., "Dynamic Stall Control for Advanced Rotorcraft Application," *AIAA Journal*, Vol. 33, No. 2, Feb. 1995, pp. 289–295. doi:10.2514/3.12496

[3] Chandrasekhara, M. S., Martin, P. B., Tung, C., "Compressible Dynamic Stall Performance of a Variable Droop Leading Edge Airfoil with a Gurney Flap," AIAA Paper 2004-0041, Reno, NV, Jan. 2004.

[4] Guzel, G., Sankar, L. N., and Rhee, M., "Computational Investigation of the Effects of Gurney Flap on the Aerodynamic Performance of VR-12 Airfoil," 23rd AIAA Applied Aerodynamics Conference, Toronto, Ontario, Canada, AIAA Paper 2005-4960, June 2005.

[5] Fulton, M., "Aeromechanics of the Active Elevon Rotor," *American Helicopter Society 61st Annual Forum* [CD-ROM], AHS International, Alexandria, VA, June 2005.

[6] Geissler, W., Sobieczky, H., "Dynamic Stall Control by Variable Airfoil Camber," *Aerodynamics and Aeroacoustics of Rotorcraft*, AGARD-CP-552, AGARD, Neuilly-sur-Seine, France, Aug. 1995, pp. 129–138.

[7] Chandrasekhara, M., "Compressible Dynamic Stall Control Using a Shape Adaptive Airfoil," 37th AIAA Aerospace Sciences Meeting, AIAA Paper 99-0650, Jan. 1999, Reno, NV.

[8] Sahin, M., Sankar, L. N., Chandrasekhara, M. S., and Tung, C., "Dynamic Stall Alleviation Using a Deformable Leading Edge Concept—A Numerical Study," *Journal of Aircraft*, Vol. 40, No. 1, Jan.–Feb. 2003, pp. 77–85. doi:10.2514/2.3060

[9] Yeo, H., "Assessment of Active Controls for Rotor Performance Enhancement," *62nd American Helicopter Society Annual Forum* [CD-ROM], AHS International, Alexandria, VA, May 2006.

[10] Chandrasekhara, M. S., Martin, P. B., and Tung, C., "Compressible Dynamic Stall Control Using a Variable Droop Leading Edge Airfoil," 41st Aerospace Sciences Meeting and Exhibit, Reno, NV, AIAA Paper 2003-48, Jan. 2003.

[11] Kerho, M., "Adaptive Airfoil Dynamic Stall Control," 43rd Aerospace Sciences Meeting and Exhibit, Reno, NV, AIAA Paper 2005-1365, Jan. 2005.

[12] Martin, P. B., McAlister, K. W., Chandrasekhara, M. S., and Geissler, W., "Dynamic Stall Measurements and Computations for a VR-12 Airfoil with a Variable Droop Leading Edge," *American Helicopter Society 59th Annual Forum* [CD-ROM], AHS International, Alexandria, VA, May 6–8, 2003.

[13] Buning, P. G., Chiu, I. T., Obayashi, S., Rizk, Y. M., and Steger, J. L., "Numerical Simulation of the Integrated Space Shuttle Vehicle in Ascent," AIAA Atmospheric Flight Mechanics Meeting, Minneapolis, MN, AIAA Paper 88-4359, Aug. 1988.

[14] Renaud, T., O'Brien, D. M., Smith, M. J., and Potsdam, M., "Evaluation of Isolated Fuselage and Rotor-Fuselage Interaction Using CFD," *American Helicopter Society 60th Annual Forum* [CD-ROM], AHS International, Alexandria, VA, June 2004.

[15] Bhagwat, M. J., Dimanlig, A., Saberi, H., Meadowcroft, E., Panda, B., and Strawn, R., "CFD/CSD Coupled Trim Solution for the Dual-Rotor CH-47 Helicopter Including Fuselage Modeling," *AHS Specialist Conference on Aeromechanics* [CD-ROM], AHS International, Alexandria, VA, Jan. 2008.

[16] Duque, E. P. N., Sankar, L. N., Menon, S., Bauchau, O., Ruffin, S., Smith, M., Ahuja, A., Brentner, K. S., Long, L. N., Morris, P. J., and Gandhi, F., "Revolutionary Physics-Based Design Tools for Quiet Helicopters," 44th AIAA Aerospace Sciences Meeting and Exhibit, Reno, NV, AIAA Paper 2006-1068, Jan. 2006.

[17] Potsdam, M., and Le Pape, A., "CFD Investigations on a NACA0036 Airfoil with Active Flow Control," 4th AIAA Flow Control Conference, Seattle, WA, AIAA Paper 2008-3869, June 2008.

[18] Bain, J., Mishra, S., Sankar, L., and Menon, S., "Assessment of a Kinetic-Eddy Simulation Turbulence Model for 3-D Unsteady Transonic Flows," 26th AIAA Applied Aerodynamics Conference, Honolulu, HI, AIAA Paper 2008-7176, Aug. 2008.

[19] Fang, Y., and Menon, S., "A Two-Equation Subgrid Model for Large-Eddy Simulation of High Reynolds Number Flows," AIAA Paper 2006-0116, Jan. 2006.

[20] Shelton, A. B., Braman, K., Smith, M. J., and Menon, S., "Improved Turbulence Modeling for Rotorcraft," *American Helicopter Society 62nd Annual Forum* [CD-ROM], AHS International, Alexandria, VA, May 2006.

[21] Spalart, P. R., and Allmaras, S. R., "A One-equation Turbulence Model for Aerodynamic Flows," AIAA Paper 92-0439, Jan. 1992.

[22] Scott, N. W., and Duque, E. P. N., "Using Detached Eddy Simulation and Overset Grids to Predict Flow Around a 6:1 Prolate Spheroid," 43rd AIAA Aerospace Sciences Meeting and Exhibit, Reno, NV, AIAA Paper 2005-1362, Jan. 2005.

[23] Kunz., D., "Comprehensive Rotorcraft Analysis: Past, Present, and Future," 46th AIAA/ASME/ASCE/AHS/ASC Structures, Structural Dynamics, and Materials Conference, Austin, TX, AIAA Paper 2005-2244, Apr. 2005.

[24] Kufeld, R. M., and Loschke, P. C., "UH-60A Airloads Program—Status and Plans," AIAA Aircraft Design Systems and Operations Meeting, Baltimore, MD, AIAA Paper 1991-3142 , Sept. 1991.

[25] Potsdam, M., Yeo, H., and Johnson, W., "Rotor Aerodynamic Prediction Using Loose Aerodynamic and Structural Coupling," *American Helicopter Society 60th Annual Forum* [CD-ROM], AHS International, Alexandria, VA, June 1994.

[26] Makinen, S., Hill, M., Gandhi, F., Long, L., Vasilescu, R., and Sankar, L., "A Study of the HART-I Rotor with Loose Computational Fluid/Structural Dynamic Coupling," *American Helicopter Society 62th Annual Forum* [CD-ROM], AHS International, Alexandria, VA, 2006.

[27] Bauchau, O. A., Bottasso, C. L., and Nikishkov, Y. G., "Modeling Rotorcraft Dynamics with Finite Element Multibody Procedures," *Mathematical and Computer Modelling*, Vol. 33, May 2001, pp. 1113–1137. doi:10.1016/S0895-7177(00)00303-4

[28] Rajmohan, N., Sankar, L., Bauchau, O., Charles, B., Makinen, S., and Egolf, T. A., "Application of Hybrid Methodology to Rotors in Steady and Maneuvering Flight," *American Helicopter Society 64th Annual Forum*, AHS International, Alexandria, VA, 2008.

[29] Tung, C., Caradonna, F. X., and Johnson, W. R., "The Prediction of Transonic Flows on an Advancing Rotor," *American Helicopter Society 40th Annual Forum*, AHS International, Alexandria, VA, 1984.

[30] Morton, S. A., Melville, R. B., and Visbal, M. R., "Accuracy and Coupling Issues of Aeroelastic Navier–Stokes Solutions on Deforming Meshes," *Journal of Aircraft*, Vol. 35, No. 5, Sept.–Oct. 1998, pp. 798–805. doi:10.2514/2.2372

[31] Bain, J., Sankar, L., Prasad, JVR, Bauchau, O., Peters, D., and He, C., "Computational Modeling of Variable Droop Leading Edge in Forward Flight," 4th Flow Control Conference, Seattle, WA, AIAA Paper 2008-3872, June 2008.

[32] Datta, A., and Chopra, I., "Prediction of UH-60A Dynamic Stall Loads in High Altitude Level Flight Using CFD/CSD Coupling," *American Helicopter Society 61st Annual Forum* [CD-ROM], AHS International, Alexandria, VA, 2005.

[33] "Dynamic Camber Control for Helicopters," U.S. Army, Small Business Innovation Research Solicitation A05-067, 2005.

[34] Bielawa, R., "Analytical Investigation of Helicopter Rotor Blade Appended Aeroelastic Devices," NASA CR 166525, 1984.